Neutron capture-induced nuclear recoils as background for CEνNS measurements at reactors

A.J. Biffl,[1,*] A. Gevorgian,[1] K. Harris,[1] and A.N. Villano[1,†]

[1] *Department of Physics, University of Colorado Denver, Denver, Colorado 80217, USA*

(Dated: May 29, 2023)

Nuclear reactors represent a promising neutrino source for CEνNS (coherent-elastic neutrino-nucleus scattering) searches. However, reactor sites also come with high ambient neutron flux. Neutron capture-induced nuclear recoils can create a spectrum that strongly overlaps the CEνNS signal for recoils $\lesssim 100\,\mathrm{eV}$ for nuclear reactor measurements in silicon or germanium detectors. This background can be particularly critical for low-power research reactors providing a moderate neutrino flux. In this work we quantify the impact of this background and show that, for a measurement 10 m from a 1 MW reactor, the effective thermal neutron flux should be kept below $\sim 7\times 10^{-4}\,\mathrm{n/cm^2 s}$ so that the CEνNS events can be measured at least at a 5σ level with germanium detectors in 100 kg yr exposure time. This flux corresponds to 60% of the sea-level flux but needs to be achieved in a nominally high-flux (reactor) environment. Improved detector resolution can help the measurements, but the thermal flux is the key parameter for the sensitivity of the experiment. For silicon detectors, the constraint is even stronger and thermal neutron fluxes must be near an order of magnitude lower. This constraint highlights the need of an effective thermal neutron mitigation strategy for future low threshold CEνNS searches. In particular, the neutron capture-induced background can be efficiently reduced by active veto systems tagging the deexcitation gamma following the capture.

I. INTRODUCTION

Coherent Elastic Neutrino Nucleus Scattering (CEνNS) is the transfer of momentum between a neutrino and a nucleus as a whole via neutral current exchange. This process is experimentally significant for detecting low energy ($\lesssim$ MeV) neutrinos due to its large cross section, two to four orders of magnitude larger than the commonly used inverse beta decay (IBD) [1, 2]. This allows CEνNS detectors to be much smaller than their IBD counterparts.

The CEνNS process has already been measured at an accelerator site by the COHERENT Collaboration using the Spallation Neutron Source at Oak Ridge National Laboratory as a neutrino source [3]. The accelerator provides neutrinos of a few tens of MeV, and other measurements using this type of source are planned, for example the upcoming European Spallation Source [2]. Likewise, recent studies show potential for measurements at reactor sites, where the sources of MeV antineutrinos are commercial or research fission reactors [4–11].

The trade-off for CEνNS' relatively high interaction rate is that it is exceptionally difficult to detect because of the tiny (sub-keV) recoil of the target nuclei, even despite recent advances in detector resolution near threshold, for example in silicon [12, 13]. One major hurdle is that distinguishing a nuclear recoil event caused by CEνNS from one caused by other sources is difficult. In the vicinity of nuclear reactors, a large reactogenic thermal neutron flux could cause enough neutron-capture-induced recoil events to hide the CEνNS signal. A capture of a neutron via the (n,γ) process produces one or more ∼MeV scale prompt gamma rays and a prompt nuclear recoil at the sub-keV scale — coinciding with the energy scale of events from reactor neutrinos.

The recoil spectrum from neutron capture on silicon has been recently measured [14] and creates nuclear recoil events down to ∼100 eV. This paper investigates the thermal neutron background mitigations needed to measure a CEνNS signal in the vicinity of a nuclear reactor.

II. CEνNS AND CAPTURE SPECTRA

We used the model given by Mueller [15] for the four principle fissionable isotopes as the model for reactor antineutrino emissions. We attempted to emulate the expected emissions of a low-enriched (∼ 20% ^{235}U) reactor fuel composition, i.e. that employed by the MINER Collaboration at the Nuclear Science Center at Texas A&M University [16]. We assume neutrino emissions consistent with the MINER study [11], i.e., dominated by ^{235}U (96.7%) with smaller fractions of ^{238}U and ^{239}Pu (1.3 and 2.0% respectively), and negligible ($\lesssim 0.1\%$) ^{241}Pu.

We tested the target materials silicon and germanium with natural isotope distributions. The reactor spectrum was convoluted with the known CEνNS cross section [2] using the form factor model given by [17] to yield a recoil energy spectrum for CEνNS events. The form factor was quite close to 1, with a largest deviation from Ge at a recoil energy of around 1 keV, where it had a value of 0.9895.

To calculate the expected recoil energy spectrum from neutron captures, we use `nrCascadeSim`, a publicly available dedicated simulation tool developed by two of the authors here for nuclear recoils resulting from neutron captures [18]. This software was used to generate a large sample of capture-induced recoil energies from which we

* Corresponding author: alexander.biffl@ucdenver.edu
† Corresponding author: anthony.villano@ucdenver.edu

construct a probability density function (PDF) to sample. The code takes into account the most probable multistep cascades in the deexcitation process following capture and the possibility of decay-in-flight for the intermediate atoms/ions within the cascade.

III. ASSUMED DETECTOR CONFIGURATION

Recoil datasets were simulated with a total of 3,000 (10,000) CEνNS events, corresponding to approximately a 100 kg yr exposure time of natural silicon (germanium) detectors, at the CEνNS event rate calculated by [11] for detector deployment 10 m from the reactor core. Events that produce energies below the detection threshold are removed when applying the resolution model. Detectors were modeled with a range of different effective resolutions (defined here as resolution σ at a recoil energy of 50 eV). All detector resolutions obeyed a resolution function of the form:

$$\sigma(E) = \sqrt{\sigma_0^2 + AE} \tag{1}$$

where E is the recoil energy, σ_0 is the baseline resolution, and A is a detector-specific factor which is varied to achieve a given effective resolution. We also consider several values of σ_0: 1 eV, 5 eV, 10 eV, and 25 eV. Table I shows resolution criteria that are either future targets or have already been achieved for several experimental efforts. We can see that the current best demonstrated solid-target baseline resolution comes from the ν-cleus Collaboration at 3.7 eV [19]–between our two lowest baseline resolution points and probably achievable in the near future for Si and Ge. Going by the table it is seen that a 25 eV baseline resolution is probably on the horizon for many detectors. For the solid detectors in the table we also see that the typical threshold is a factor of 3–9 larger than the baseline resolution–roughly in line with our requirement that events have energies $\geq 5\sigma_0$ (see below).

Different levels of ambient thermal neutron flux were surveyed between about $\sim 10^{-7}$ n/cm^{2}sand $\sim 10^{-3}$ n/cm^{2}s. The flux range is motivated by where this analysis produces high significance (5σ) in the presence of modest "other" background (see below). The flux range includes the approximate behavior of the Dresden-II [4] published thermal neutron flux — 0.25 n/cm^{2}s— if we account for an approximately 3000 times higher reactor output power of that commercial reactor. The fluxes were translated to a total capture event count via the neutron capture cross section with natural silicon and germanium and assuming an exposure of 100 kg yr. The capture events were then sampled from the output PDF of `nrCascadeSim v1.4.2`. All sampled recoils with energy $\leq 5\sigma_0$ were eliminated to emulate data collection with a finite energy threshold event trigger.

Thermal neutrons are not the only nuclear recoil backgrounds possible in CEνNS experiments, so we include an "other" nuclear recoil background with shape

Experiment	Detector type	Threshold	Baseline resolution
CONNIE[20, 21]	Si CCD	28 eVee[b]	5.5 eVee[b]
CONUS[22]	Ge PPC	200 eVee[b]	25 eVee[b]
Dresden-II[4]	Ge PPC	200 eVee[b]	33 eVee[b]
MINER[11]	Si/Ge cal	$\sim$ 20 eV[a]	5 eV[a]
RED-100[23, 24]	Xe 2PS	300 eV[a]	···
RICOCHET[25, 26]	Si/Ge bol	$\sim$ 50 eV[a]	17 eV[b]
TEXONO[27, 28]	Ge PPC	300-400 eVee[a]	45 eVee[b]
ν-cleus[19]	$CaWO_4$ / Al_2O_3 cal	19.7 eV[b]	3.7 eV[b]
νGeN[29]	Ge PPC	350 eV[b]	93 eV[b]

TABLE I. Summary of CEνNS searches at reactors. Non-standard abbreviations used are as follows. **cal**: Calorimeter. **2PS**: Two-phase scintillator. **bol**: Bolometer. Note also eVee refers to electron-equivalent (ionization) energy; other energies are heat.

[a] target
[b] achieved

$\propto E^{-0.9}$, consistent with neutron-scatter background data given by [16], and very similar to the $E^{-1.2}$ form mentioned in [5]. From MINER's 2017 background measurement they expect a combined 100 events/kg/day in nuclear recoil and electron recoil backgrounds but only 5-20 events/kg/day in CEνNS events [16]. The MINER authors acknowledge the need to control background and other experiments have demonstrated backgrounds with between 40-60% of what is expected from the CEνNS process [10, 30]. Given this information we normalize our nuclear recoil background to 60% of the CEνNS rate below about 1 keV. We do not add any further electron recoil background because it is often diluted to higher electron equivalent energies in ionization-sensitive detectors. Furthermore, the electron recoils in some cases can be discriminated [31–33]. This background model is expected to represent approximately the maximum acceptable background to a typical CEνNS search. Other variations of our fits have been completed in the release of our code for this analysis [34].

IV. STATISTICAL COMPARISON

The combined sample of recoil energies from the three sources (CEνNS, neutron capture, and other backgrounds), were separated back into CEνNS and neutron-capture components by binned maximum-likelihood fits with the likelihood function:

$$\mathcal{L} = e^{-n_{\text{total}}} \prod_{j=1}^{N_{\text{bins}}} \frac{1}{C_j!} \left[n_\nu P_{\nu,j} + n_c P_{c,j} + n_b P_{b,j} \right]^{C_j}, \tag{2}$$

where C_j is the observed number of events in bin j, n_ν, n_c, and n_b are the fitted number of CEνNS, capture, and background events, respectively, n_{total} is the sum of these, and $P_{\nu,j}$, $P_{c,j}$, and $P_{b,j}$ are the probability of an

event of each type lying in bin j (all normalized such that they sum to unity over all bins).

We employ a likelihood ratio test on $\mathcal{L}/\mathcal{L}'$, where $\mathcal{L}'$ is a similar likelihood function but without the CEνNS contribution–with the parameter n_ν in Eq. (2) set to zero.

The two likelihoods are compared using Wilks' theorem, which states that $2\ln(\mathcal{L}/\mathcal{L}')$ is distributed as a chi-squared random variable with, in this case, one degree of freedom [35]. This leads immediately to a probability for comparing the nested models, i.e., the probability that the combined model of Eq. (2) *is* a better model than the simple model with $n_\nu \equiv 0$. We quantify the *confidence level* as the Z-value (σ value) corresponding to the symmetric (two-sided) normal error integral with the same probability, i.e., $\sqrt{2\ln(\mathcal{L}/\mathcal{L}')}$.

Figure 1 shows example fits for different combinations of effective resolutions and neutron fluxes in silicon. Resolutions of 10 eV and 35 eV are used in conjunction with neutron fluxes of 4.36×10^{-5} n/cm^{2}s and 9.77×10^{-5} n/cm^{2}s with $\sigma_0 = 1$ eV. The black points show the histogram of our toy model data for given CEνNS, thermal flux, and background contributions. The toy model data is smeared using our hypothetical resolution functions and plotted for recoil energies between 0 eV and 1800 eV. Solid blue and orange curves show the fitted PDFs for with- and without-CEνNS fits. The dashed blue curve shows the CEνNS contribution to the with-CEνNS fit. The confidence level of each fit is given in the upper left corner of each plot, red if less than 5σ and blue if greater.

In Figure 1 the leftmost and rightmost plots show the two methods by which the CEνNS signal can be detected, either by improving resolution so the CEνNS signal can be discerned on the low-energy downslope (leftmost plot), or by reducing the neutron flux so that the peak caused by CEνNS events is clearly visible over the signal from capture events (rightmost plot). The center plot shows a scenario where the thermal neutron flux is too high to produce a 5σ CEνNS detection with the assumed livetime. Figure 2 shows the analogous fit plots for germanium. In the germanium case we use resolutions of 20 eV and 45 eV with thermal neutron fluxes of 5.52×10^{-4} n/cm^{2}s and 1.75×10^{-4} n/cm^{2}s. The thermal neutron fluxes used for germanium are generally higher than for silicon because germanium is more resilient to the flux — although there are more capture events the capture spectrum overlaps less strongly than in silicon.

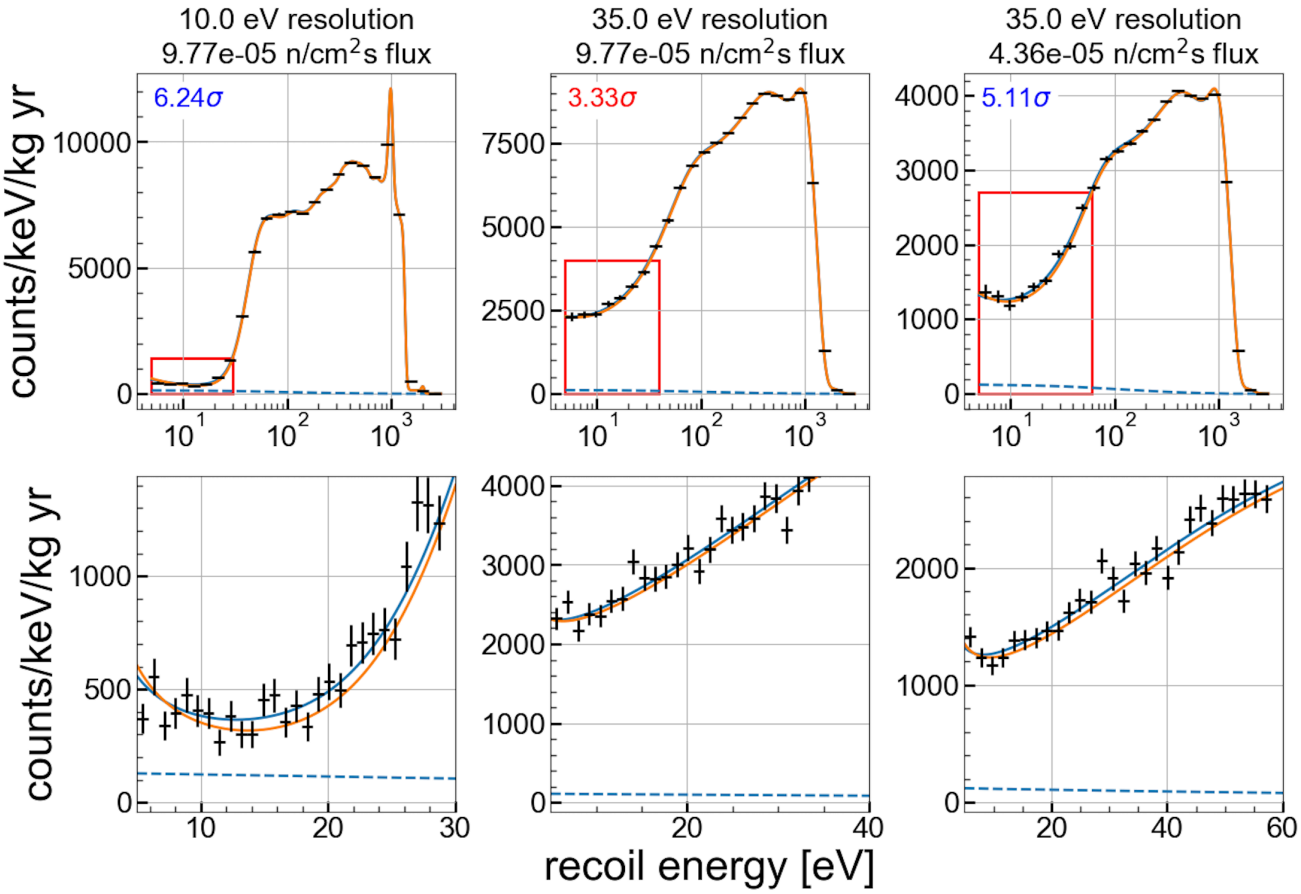

FIG. 1. (Color online) Likelihood fitting examples for three different combinations of resolution and neutron flux for $\sigma_0 = 1\,\mathrm{eV}$ in silicon. The left two plots show a flux of 9.77×10^{-5} n/cm^{2}s, corresponding to $\sim 1.1\,\mathrm{M}$ capture events, and the right is lower flux, 4.36×10^{-5} n/cm^{2}s, corresponding to $\sim 500,000$ capture events. The right two plots show data with an effective resolution of 35 eV, and the left plot shows an effective resolution of 10 eV. The black points show the histogram of our toy model data for given CEνNS, thermal flux, and background contributions. Solid blue and orange curves show the fitted PDFs for with- and without-CEνNS fits. The dashed blue curve shows the CEνNS contribution to the with-CEνNS fit.

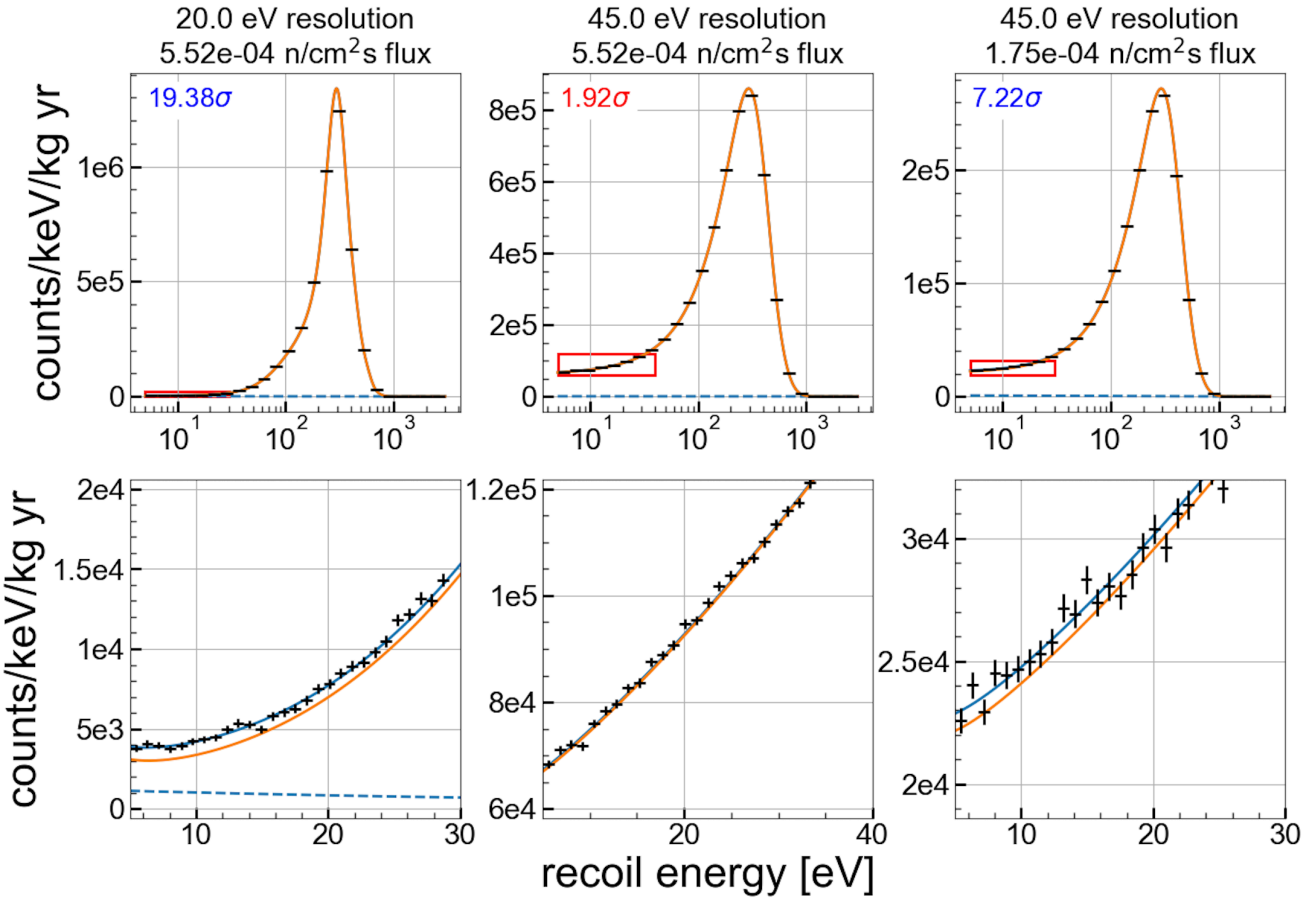

FIG. 2. (Color online) Likelihood fitting examples for three different combinations of resolution and neutron flux for $\sigma_0 = 1\,\text{eV}$ in germanium. The left two plots show a flux of 5.52×10^{-4} n/cm^{2}s, corresponding to $\sim 31.6\,\text{M}$ capture events, and the right is lower flux, 1.75×10^{-4} n/cm^{2}s, corresponding to $\sim 10\,\text{M}$ capture events. The right two plots show data with an effective resolution of 45 eV, and the left plot shows an effective resolution of 20 eV. The black points show the histogram of our toy model data for given CEνNS, thermal flux, and background contributions. Solid blue and orange curves show the fitted PDFs for with- and without-CEνNS fits. The dashed blue curve shows the CEνNS contribution to the with-CEνNS fit.

V. RESULTS AND DISCUSSION

Figure 3 shows the results for 100 kg yr exposure in Si (left) and Ge (right) for $\sigma_0 = 1\,\text{eV}$. To produce this plot, we generated a grid of 25 resolution values and 25 flux values and completed fits on that grid for each material. The contour plot is a smoothing of those fit results. The vertical axis shows ambient thermal neutron flux and the horizontal axis shows the effective resolution. Colors correspond to confidence levels. The two horizontal broken lines delineate a few reference flux levels — the gray dashed line shows the generally accepted ambient neutron flux at sea level, 4 cm^{-2} hr^{-1} [36]. The gray dotted line shows 1 part in 10^9 of the neutron flux measured at the MINER facility, $5.8{\times}10^7$ $\text{cm}^{-2}\,\text{s}^{-1}$ [16], extrapolated to ten meters from the reactor core. As reference, the two lines correspond to approximately 13,000,000 (63,000,000) and 7,500,000 (37,000,000) neutron capture events in Si (Ge), respectively.

The black lines represent 5σ contours, approximately 99.99994% confidence in the presence of the CEνNS signal, for three different values of σ_0 (the 1 eV contour is the contour for the pictured colormap data). Each contour was yielded after smoothing the data by six iterations through a Jacobi relaxation scheme. Above each line, it is unlikely that the CEνNS signal can be extracted from the data given that baseline resolution.

Up to statistical fluctuations, the confidence increases monotonically moving toward lower fluxes and better resolutions, as would be expected. This is the case for all baseline resolutions probed.

Many interesting features can be seen in this data. For $\sigma_0 = 1\,\text{eV}$, below an effective resolution of $\sim 20\,\text{eV}$, improving resolution has a dramatic effect on tolerance to ambient neutrons. An improvement in effective resolution from 10 eV to 20 eV is enough to allow measurement of CEνNS in an ambient flux three times larger. However, at larger baseline resolutions, the improvement with effective resolution is much smaller, and at $\sigma_0 = 10$ eV, changing the effective resolution does almost nothing. This is an instructive, and promising, result, emphasizing that the feasibility of CEνNS measurements gets ever greater as detector technologies improve, but that decreasing the thermal neutron flux of current experiments may be a vital step in achieving these measurements.

Further, even with drastic detector improvements, thermal neutrons could still represent a substantial background in the vicinity of nuclear reactors. It can be seen in Figure 3 that the measured MINER reactor-adjacent flux needs to be brought down to one part in a billion to begin seeing a CEνNS signal at a baseline resolution of only 1 eV, and must be brought down even further at $\sigma_0 = 10\,\text{eV}$. Note that the flux measurement by MINER [16] was early in the campaign. Many materials like boron, cadmium, gadolinium, polyethylene, and more can be used to bring down thermal fluxes by large factors. The thermal neutron background situation is somewhat better in germanium detectors owing to the larger CEνNS cross section and lower capture rates at low energy.

We have done our analysis in terms of nuclear recoil energies but many detectors will measure the ionization caused by nuclear recoils instead. This will tend to shift all the nuclear recoil events toward lower energies, as the ionization yield is below unity and typically lower at lower energies [37]. However, we expect our results to be unaffected as the shift is largely the same for both capture and neutrino induced recoils. The resolution and detector threshold would also have to be adapted to the specific case.

In germanium detectors the thermal neutron flux can be measured *in situ* and compared with our results. The flux measurement is based on the rates of one of the X-ray emissions from electron capture of ^{71}Ge. After several half-lives ($T_{1/2}$=11.4 days) the ambient neutron flux will be equal to the rate of the K-shell electron capture (EC) line divided by a quantity which is the product of the branching of that line, the macroscopic cross section of ^{70}Ge capture, and the volume of the detector.

Thus far, this study has not discussed the possibility of vetoing events based on outgoing capture gamma rays. In general, capture events are highly vetoable by looking for signs of the gammas emitted during each capture. As a simple estimate of plausible effective flux reduction, Table II lists the expected effective flux $f_{\text{effective}}$ over the actual flux f_{actual} as a function of $\bar{d}$, the angle-weighted average distance an emitted gamma would travel before leaving a detector made of either silicon or germanium. Values are based on the probability of gammas from capture event leaving the detector without interacting, based on the same cascades (potentially involving multiple exiting gamma rays) and cascade rates used to generate the capture event spectra, and using gamma/nucleus cross sections yielded via linearly interpolating data from NIST's XCOM database [38]. These estimates show that physically larger detectors can make great gains in reducing the importance of ambient thermal neutrons, particularly in the case of germanium.

	$f_{\text{effective}}/f_{\text{actual}}$	
$\bar{d}$ (cm)	Si	Ge
1	0.8382	0.442
5	0.4267	0.07027
10	0.1937	0.01251
20	0.04538	0.001166
50	0.001747	7.313e-06
100	7.119e-05	1.917e-09

TABLE II. Expected effective thermal neutron flux $f_{\text{effective}}$ over actual flux f_{actual} in silicon and germanium detectors as a function of $\bar{d}$, the average distance a gamma must travel before leaving the detector. Reduction is based on the probability of gammas leaving the detector without interacting.

Some assumptions about the "other" backgrounds should be noted. The low-energy-skewed spectrum ($\propto E^{-0.9}$) can be viewed as an instantiation of the anomalous excess of events in low-threshold cryogenic de-

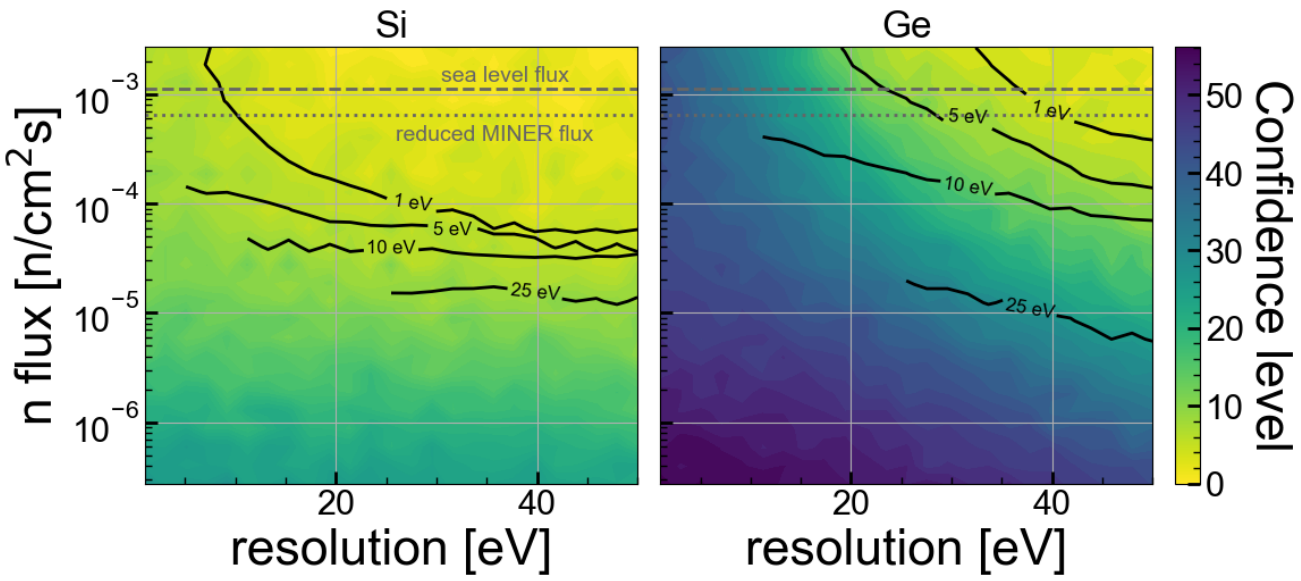

FIG. 3. (Color online) Confidence level for varying ambient thermal neutron flux (vertical axis) and effective resolution (horizontal axis) for a baseline resolution of 1 eV in Si (left) and Ge (right). Horizontal lines mark fluxes corresponding the accepted ambient sea level flux (dashed) and one part in 10^9 of the measured flux at the MINER facility [16] (dotted). Black contour lines representing 5σ confidence levels for different values of the baseline resolution σ_0 are also shown. The value of σ_0 corresponding to each contour is given by the label on each contour.

tectors at low energy recently measured by several collaborations [16, 30, 39–50]. The origin of these events are unclear, and a single common explanation for the excesses is unlikely, making it difficult to assess the likely form for such an excess in our simulated experiment. However, since we consider the nuclear recoil energy scale these excess events are either similarly peaked to our assumed additional background model, or they are more spread out due to the less-than-unity quenching factor of nuclear recoils.

The last point that bears discussion is that the reactor model used here may be a best-case scenario. A parallel track of calculations in silicon using antineutrino spectrum data from the Daya Bay nuclear reactor complex in Southern China [51] yielded consistently lower confidence values. This fact highlights possible systematic uncertainties in our analysis due to uncertainties in the reactor anti-neutrino spectrum. The precise shape and overall normalization of this spectrum is actively being improved [52, 53], but the current status does not preclude changes to our results based on the form of the spectrum. This is expected to be a more significant effect than changes based on uranium enrichment and relative fission contributions from ^{235}U, ^{238}U, ^{239}Pu, and ^{241}Pu. This is certainly a less significant effect than the ability to veto capture events, but still should be noted.

Overall, our analysis shows that keeping the effective thermal neutron flux (flux after veto) below $\sim 10^{-4}$ n/cm^{2}s for a 1 MW reactor at 10 meters is necessary for silicon detectors–even ones with exceptional resolutions. Germanium is somewhat more robust for detectors with exceptional resolution, requiring the flux to be below $\sim 7{\times}10^{-4}$ n/cm^{2}s under the same conditions. For germanium detectors with 25 eV baseline resolution (still excellent by today's standards) the thermal neutron flux needs to fall below $\sim 10^{-5}$ n/cm^{2}s. These rules of thumb can be roughly adapted to other reactors by multiplying this flux by the reactor power in MW (uranium enrichment level probably makes a sub-dominant difference) and accounting for the distance by an inverse-square law for the neutrinos.

All of the Python code used for this analysis can be obtained via the Open Storage Framework (OSF) data entry [34]. The PDFs for the thermal neutron-induced nuclear recoils were obtained from our public code [18].

ACKNOWLEDGMENTS

We gratefully acknowledge support from the U.S. Department of Energy (DOE) Office of High Energy Physics and from the National Science Foundation (NSF). This work was supported in part by DOE Grant DE-SC0021364 and NSF Grant No. 2111090.

[1] A. Oralbaev, M. Skorokhvatov, and O. Titov, Journal of Physics: Conference Series **675**, 012003 (2016).
[2] D. Baxter *et al.*, Journal of High Energy Physics **2020**, 10.1007/jhep02(2020)123 (2020).
[3] D. Akimov *et al.*, Science **357**, 1123 (2017).
[4] J. Colaresi, J. I. Collar, T. W. Hossbach, A. R. L. Kavner, C. M. Lewis, A. E. Robinson, and K. M. Yocum, Phys. Rev. D **104**, 072003 (2021).
[5] J. Colaresi, J. I. Collar, T. W. Hossbach, C. M. Lewis, and K. M. Yocum, Phys. Rev. Lett. **129**, 211802 (2022).
[6] A. Aguilar-Arevalo *et al.* (CONNIE), JHEP **05** (17), 017, arXiv:2110.13033 [hep-ex].
[7] H. Bonet *et al.* (CONUS Collaboration), Phys. Rev. Lett. **126**, 041804 (2021).
[8] I. Alekseev *et al.* (νGeN collaboration), Phys. Rev. D **106**, L051101 (2022).
[9] G. Angloher *et al.* (NUCLEUS), Eur. Phys. J. C **79**, 1018 (2019), arXiv:1905.10258 [physics.ins-det].
[10] Ricochet Collaboration, G. Beaulieu, *et al.*, Ricochet progress and status, arXiv:2111.06745 (2021).
[11] W. E. Ang, S. Prasad, and R. Mahapatra, Nuclear Instruments and Methods in Physics Research Section A: Accelerators, Spectrometers, Detectors and Associated Equipment **1004**, 165342 (2021).
[12] R. K. Romani *et al.*, Applied Physics Letters **112**, 043501 (2018).
[13] J. Tiffenberg *et al.*, Phys. Rev. Lett. **119**, 131802 (2017).
[14] A. N. Villano, M. Fritts, N. Mast, S. Brown, P. Cushman, K. Harris, and V. Mandic, Phys. Rev. D **105**, 083014 (2022).
[15] T. A. Mueller *et al.*, Phys. Rev. C **83**, 054615 (2011).
[16] G. Agnolet *et al.*, Nuclear Instruments and Methods in Physics Research Section A: Accelerators, Spectrometers, Detectors and Associated Equipment **853**, 53 (2017).
[17] S. R. Klein and J. Nystrand, Phys. Rev. C **60**, 014903 (1999).
[18] A. Villano, K. Harris, and S. Brown, Journal of Open Source Software **7**, 3993 (2022).
[19] R. Strauss *et al.*, Phys. Rev. D **96**, 022009 (2017).
[20] A. Aguilar-Arevalo *et al.* (CONNIE Collaboration), Phys. Rev. D **100**, 092005 (2019).
[21] G. Fernandez Moroni, J. Estrada, E. E. Paolini, G. Cancelo, J. Tiffenberg, and J. Molina, Phys. Rev. D **91**, 072001 (2015).
[22] H. Bonet *et al.*, The European Physical Journal C **82**, 10.1140/epjc/s10052-022-10722-1 (2022).
[23] D. Y. Akimov *et al.*, Physics-Uspekhi **62**, 166 (2019).
[24] D. Akimov *et al.*, Journal of Instrumentation **15** (02), P02020.
[25] J. A. Formaggio, E. Figueroa-Feliciano, and A. J. Anderson, Phys. Rev. D **85**, 013009 (2012).
[26] A. Leder *et al.*, Journal of Instrumentation **13** (02), P02004.
[27] M. K. Singh *et al.*, Indian Journal of Physics **91**, 1277–1291 (2017).
[28] M. K. Singh *et al.*, Chinese Journal of Physics **58**, 63 (2019).
[29] V. Belov *et al.*, Journal of Instrumentation **10** (12), P12011.
[30] J. Billard *et al.*, Journal of Physics G: Nuclear and Particle Physics **44**, 105101 (2017).
[31] H. Neog *et al.*, Nuclear Instruments and Methods in Physics Research Section A: Accelerators, Spectrometers, Detectors and Associated Equipment **1033**, 166707 (2022).
[32] H. Lee *et al.*, Journal of High Energy Physics 10.1007/JHEP08(2015)093 (2015).
[33] W.-Z. Wei, J. Liu, and D.-M. Mei, Journal of Instrumentation **11** (07), P07008.
[34] A. N. Villano, A. Biffl, and K. Harris, Neutron capture-induced nuclear recoils as background for CEvNS measurements at reactors, 10.17605/OSF.IO/7682T (2023).
[35] S. S. Wilks, Annals Math. Statist. **9**, 60 (1938).
[36] J. Dirk, M. Nelson, J. Ziegler, A. Thompson, and T. Zabel, IEEE Transactions on Nuclear Science **50**, 2060 (2003).
[37] J. Lindhard, V. Nielsen, M. Scharff, and P. Thomsen, Kgl. Danske Videnskab., Selskab. Mat. Fys. Medd. **33**, 31 (1963).
[38] M. J. Berger, J. H. Hubbell, S. M. Seltzer, J. Chang, J. S. Coursey, R. Sukumar, D. S. Zucker, and K. Olson, XCOM: Photon cross section database (version 1.5), `http://physics.nist.gov/xcom` (2010), published by the National Institute of Standards and Technology (NIST), Gaithersburg, MD. Accessed 2021-12-08.
[39] P. Adari *et al.*, SciPost Phys. Proc. , 001 (2022).
[40] A. Aguilar-Arevalo *et al.* (CONNIE), Journal of Physics: Conference Series **761**, 012057 (2016).
[41] A. H. Abdelhameed *et al.* (CRESST Collaboration), Phys. Rev. D **100**, 102002 (2019).
[42] A. Aguilar-Arevalo *et al.* (DAMIC Collaboration), Phys. Rev. Lett. **125**, 241803 (2020).
[43] E. Armengaud *et al.* (EDELWEISS Collaboration), Phys. Rev. D **99**, 082003 (2019).
[44] Q. Arnaud *et al.* (EDELWEISS Collaboration), Phys. Rev. Lett. **125**, 141301 (2020).
[45] Q. Arnaud *et al.*, Astroparticle Physics **97**, 54 (2018).
[46] J. Rothe *et al.* (NUCLEUS Collaboration), Journal of Low Temperature Physics **199**, 433 (2020).
[47] L. Barak *et al.* (SENSEI Collaboration), Phys. Rev. Lett. **125**, 171802 (2020).
[48] D. W. Amaral *et al.* (SuperCDMS Collaboration), Phys. Rev. D **102**, 091101 (2020).
[49] I. Alkhatib *et al.* (SuperCDMS Collaboration), Phys. Rev. Lett. **127**, 061801 (2021).
[50] R. Agnese *et al.* (SuperCDMS Collaboration), Phys. Rev. Lett. **121**, 051301 (2018).
[51] F. P. An *et al.*, Chinese Physics C **41**, 013002 (2017).
[52] A. C. Hayes and P. Vogel, Annual Review of Nuclear and Particle Science **66**, 219 (2016).
[53] M. Estienne *et al.*, Phys. Rev. Lett. **123**, 022502 (2019).